Materiales de Construcción
Vol. 72, Issue 346, April-June 2022, e281
ISSN-L: 0465-2746
https://doi.org/10.3989/mc.2022.15621

Investigations on alkali-silica reaction products using Raman spectroscopy

M.E. Krüger[a]✉, V. Thome[b], H. Hilbig[a], M. Kaliwoda[c], D. Heinz[a]

a. Centre for Building Materials (CBM), Technical University of Munich, (Munich, Germany)
b. Fraunhofer Institute for Building Physics (IBP), (Valley, Germany)
c. Mineralogical State Collection Munich, SNSB, (Munich, Germany)
✉: miriam.krueger@tum.de

Received 23 October 2021
Accepted 13 March 2022
Available on line 29 April 2022

ABSTRACT: The alkali–silica reaction (ASR) remains a major challenge regarding the durability of concrete structures. The reaction mechanism is not sufficiently understood owing to the difficulty in characterizing the structure of the alkali-silica reaction gel (ASR gel) in concrete. Synthetic ASR gels with different compositions, i.e. Na/Si and Ca/Si molar ratios, were synthesized and analysed by Raman spectroscopy and, for comparison, ^{29}Si NMR spectroscopy. The results show that higher Na/Si ratios increase the number of non-bridging oxygens in the gel structure, thus leading to a decrease in the degree of cross-linking. With increasing calcium content of the sodium-calcium silica gel, the structure tends towards that of C-S-H phases. Raman spectroscopy is a promising method to characterise synthetic ASR gels and provide new information on the effect of alkalis on the gel structure.

KEYWORDS: Alkali-silica reaction (ASR); Alkali-silica reaction gel (ASR gel); Raman spectroscopy; ^{29}Si NMR spectroscopy; Concrete.

Citation/Citar como: Krüger, M.E.; Thome, V.; Hilbig, H.; Kaliwoda, M.; Heinz, D. (2022) Investigations on alkali-silica reaction products using Raman spectroscopy. Mater. Construcc. 72 [346], e281. https://doi.org/10.3989/mc.2022.15621.

RESUMEN: *Investigaciones sobre productos de reacción álcali-sílice mediante espectroscopia Raman.* La reacción álcali-sílice (RAS) sigue siendo un reto importante para la durabilidad de las estructuras de hormigón. El mecanismo de reacción de la RAS aún no está suficientemente aclarado debido a la dificultad para caracterizar la estructura del gel de reacción álcali-sílice (gel RAS) en el hormigón. Se sintetizaron geles de RAS con diferentes composiciones, es decir, con proporciones molares de Na/Si y Ca/Si, y se analizaron mediante espectroscopia Raman y se validaron comparando los resultados con mediciones espectroscópicas de RMN de ^{29}Si. Los resultados muestran que las relaciones Na/Si más elevadas aumentan el número de oxígenos no puente en la estructura del gel, lo que conduce a una disminución del grado de reticulación. Al aumentar el contenido de calcio del gel de sílice sódico-cálcico, la estructura se asemeja más a la de las fases C-S-H. La espectroscopia Raman es un método prometedor para caracterizar los geles sintéticos de RAS y proporciona nueva información sobre el efecto de los álcalis en la estructura del gel.

PALABRAS CLAVE: Reacción álcali-sílice (RAS); Gel de reacción álcali-sílice (gel RAS); Espectroscopía Raman; Espectroscopía de RMN de ^{29}Si; Hormigón.

This article was selected among the papers presented at the 2022 *International Conference on Alkali-Aggregate Reaction in Concrete* (16th ICAAR)

1. INTRODUCTION

The alkali-silica reaction (ASR) is a major cause of concrete deterioration. During ASR, alkali-reactive siliceous aggregates react with the alkalis in the pore solution of the concrete to form an expansive alkali-silica reaction gel (ASR gel). Due to its hygroscopic behaviour, the ASR gel absorbs water and swells resulting in pressures often leading to a typical crack-network-pattern with a severe impact on concrete durability.

The chemical composition of ASR gels in concretes mentioned in literature varies between molar (K+Na)/Si ratios of 0.1 to 0.7 and Ca/Si ratios of 0.2 to 0.6 (1-3). The variation in the chemical composition of the ASR gel makes it difficult to assign a uniform structural description to the gels. In the literature, ASR products are distinguished by two main types, i.e. amorphous and crystalline ASR products (1, 4, 5).

The crystalline ASR products show similarities to the mineral shlykovite [$KCa[Si_4O_9(OH)]\cdot 3H_2O$]. The structure of the crystalline ASR products consists of silicate sheets and is dominated by Q^3 species (5, 6). However, it is thought that crystalline ASR products, as opposed to the amorphous products, do not lead to damage in concrete (7). Thus this study focuses on the amorphous ASR products.

The nanostructure of amorphous ASR gels can be considered as irregular cross-linked SiO_4^{4-} tetrahedra. Hou (8) described the structure of synthetic ASR gels as low-order Q^3-dominated layers. The surface of the ASR gel is in thermodynamic equilibrium with dissolved cations (K^+, Na^+ and Ca^{2+}) which are chemically bonded as surface groups (e.g. ≡Si–ONa). According to (9, 10), the structure of the ASR gel is comparable to the structure of kanemite [$NaSi_2O_5\cdot 3H_2O$]. However, the structure of the ASR gel is more complex due to its higher water absorption capacity which lead to greater swelling pressures than kanemite (10).

The swelling behaviour of the ASR gels is controlled by their calcium content. Mansfeld (11) classified the swelling capacity of natural and synthetic ASR gels according to calcium content. Only gels with a calcium oxide content between 5 and 30 wt.% (e.g. Ca/Si molar ratio = 0.07 – 1.27) are able to develop damaging swelling pressures. ^{29}Si NMR spectroscopic studies on synthetic ASR products have shown that in the presence of calcium, resonances corresponding to Q^1 and Q^2 sites can occur, similar to those observed in C-S-H phases (2). According to Leemann et al. (2) the amount of Q^2 sites in the structure of synthetic ASR products increases with increasing Ca/Si molar ratio.

In the case of concrete, a sufficient amount of ASR gel cannot be obtained experimentally to characterize the gel with the usual laboratory methods. However, Raman spectroscopy enables the fast investigation of small sample quantities, without preparation and at a better cost effectiveness. A number of authors have confirmed the suitability of Raman spectroscopy for assigning Q-species to the structure of ASR gels (1, 12, 13).

The present study investigates the effect of different compositions on the structure of synthetic ASR gels. Raman spectroscopic measurements were performed on synthetic ASR gels with different compositions, i.e. Na/Si and Ca/Si molar ratios. The Raman spectra were evaluated with the PeakFit software and compared with data from the literature and in-house databases specID and MSC-RD (14). The band assignments were validated by comparing the results with ^{29}Si NMR spectroscopic measurements.

2. METHODS

2.1. Synthesis of ASR gels

The ASR gels were synthesized from the following starting materials: $Ca(OH)_2$, colloidal SiO_2 (40 % suspension in H_2O), deionized water and NaOH or KOH pellets. The NaOH or KOH was dissolved in the deionized water and the colloidal SiO_2 and the $Ca(OH)_2$ were then added. Six blends were prepared at room temperature in high-density polyethylene bottles and stored for three weeks in an overhead rotating mixer at a mixing speed of twelve revolutions per minute. After mixing, a portion of the sediment was removed and dried in a vacuum desiccator for seven days. It was not possible to prevent a small degree of carbonation. The sample designations and compositions are listed in Table 1. The exact molar ratios of the synthetic and dried ASR gels were determined by ICP-OES.

2.2. Raman spectroscopy

The measurements were carried out with a Raman spectrometer Senterra I (Bruker) at the Fraunhofer IBP, Valley, Germany. The Raman spectrometer is

Table 1. Molar ratios of synthetic ASR gel.

Sample name	Na/Si	K/Si	Ca/Si
	Molar ratio		
KS0.3	-	0.30	
NS0.3	0.30	-	-
NS0.6	0.60	-	-
NS1.2	1.20	-	-
NSC0.3_0.22	0.30	-	0.22
NSC0.7_0.46	0.70		0.46

equipped with an Olympus BX 51 confocal polarizing microscope. The samples were measured using frequency doubled Nd: YAG laser with a wavelength of 532 nm, a maximum laser power of 10 - 20 mW and 20x objective lens (laser diameter 5 µm). The measuring process was carried out with the software OPUS 7.5. The measurements were performed in a spectral range of 50 - 4000 cm^{-1} with a spectral resolution of 2 cm^{-1}. At least five measurements were carried out at different positions on each sample. During each measurement, a background correction and spike suppression were applied. The measured spectra were processed with using a baseline correction and a smoothing function. The phase assignments of the Raman spectra were performed by comparison with recorded spectra of the databases specID and MSC-RD (14). The Raman spectra were evaluated using the program PeakFit (version 4.06, Systat Software, Inc.). The R^2 values of the fitted Raman data ranged between 0.99 - 0.999. The settings for the evaluation are listed in Table 2.

Table 2. Basic settings for the evaluation of the Raman spectra with the program Peakfit.

Derivation	I. (first)	Peak type	Gauss+Lor Amp
Baseline correction	Hyperbolic, D2	Add residues	✔
Tol.%	max. 3,0 %	Vary width	✔
Smoothing	Savitsky-Golay	Vary shape	✔

2.3. ^{29}Si NMR spectroscopy

The ^{29}Si NMR experiments were performed with a Bruker Avance 300 spectrometer (magnetic field strength 7.0455 T, resonance frequency for ^{29}Si: 59.63 MHz) in MAS mode (magic angle spinning) using the single pulse technique (90° pulse). The samples were placed in 4 mm zirconia rotors and spun at 8 kHz. About 5000 scans were recorded for each spectrum with a repetition time of 45 s. The chemical shifts were set relative to the external standard tetramethylsilane. The signal patterns of the spectra were deconvoluted with Bruker WINNMR software.

3. RESULTS AND DISCUSSION

The vibrational band assignments of Raman spectra are listed in Table 3. In general, the results of Raman and ^{29}Si NMR spectroscopy show that the synthetic ASR gels have a disordered silicate framework with different degrees of connectivity of the silicate units (Q^n).

3.1. Synthetic silica gels without calcium

Two characteristic Raman peak pattern of the sample KS0.3 are illustrated in Figure 1. The vibrational bands in the ranges 400 - 650 cm^{-1} and 850 - 1200 cm^{-1} correspond to Si-O-Si and Si-O bonds, respectively. The evaluation of Si-O-Si group reveals one main peak at 533 cm^{-1} for Q^3 sites (17). The small peak at 431 cm^{-1} is characteristic for SiO_4 tetrahedra vibration of Q^4 sites and the peak at 462 cm^1 corresponds to symmetric bending (SB) vibration of O_{NBO}-Si-O_{NBO} (15, 16). At 597 cm^{-1}, there is one SB vibration band, which is attributed to Q^2 sites (17). The dominant peak for Q^3 silicate sites at

Table 3. Vibrational band assignments of Raman spectra (cm^{-1}) of the synthetic ASR gels (NBO: non-bridging oxygen, SB: symmetric bending, SS: symmetric stretching).

KS0.3	NS0.3	NS0.6	NS1.2	NSC0.3 _0.22	NSC0.7 _0.46	Assignments	Ref.
462	452	450	447	450	446	O_{NBO}-Si-O_{NBO} bending	(15, 16)
533	530	548	551	584	601*	SB Si-O-Si of Q^3 units	(17)
597	596	600	600	603*	630	SB Si-O-Si of Q^2 units	(17)
-	-	-	-	657	669	SB Si-O-Si of Q^2 units for C-S-H	(15, 18)
779	780	780	776	784	772	Si against tetrahedral O motion	(12)
897	900	921	928	892	930	SS Si-O (Q^1)	(12, 19)
990	985	984	994	984	996	SS Si-O (Q^2)	(12, 17)
1040	1041	1042	-	1027*	1035	SS Si-O (Q^3)	(12)
1065	1065	1068	1067	1065	1065	v_1 [CO_3^{2-}]	(12, 20)
3415	3420		3397	3407	3415	OH stretching	(15, 18)

***Q^2 or Q^3 units**

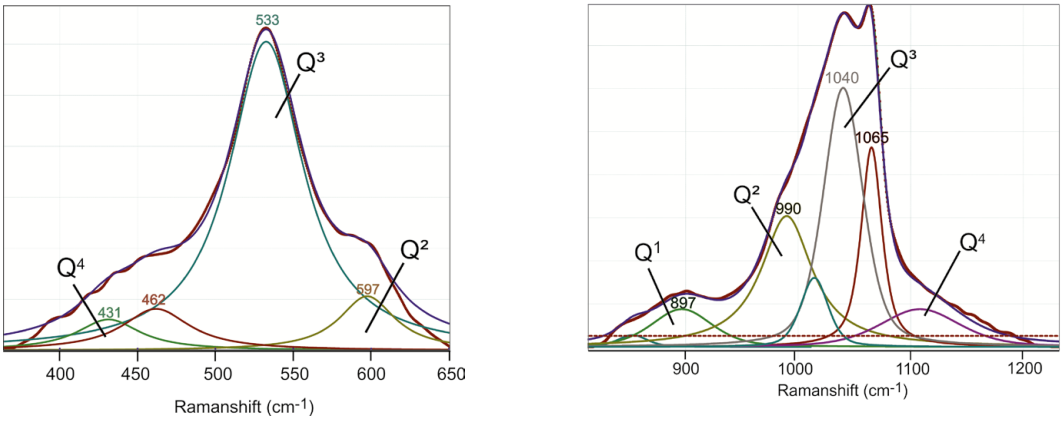

FIGURE 1. Two main vibrational peak pattern at 400 - 650 cm-1 and 850 -1200 cm-1 for the sample KS0.3 (potassium silica gel, K/Si molar ratio = 0.3).

1040 cm^{-1} corresponds to symmetric stretching (SS) vibration. The SS vibrational peak at 990 cm^{-1} is linked to Q^2 sites. The flat and broad band at 897 cm^{-1} is related to the symmetric stretching vibration of Q^1 sites (12, 17). The peak position at 1065 cm^{-1} can be linked to CO_3^{2-} vibration (12, 20). The peak position at 1108 cm^{-1} can be assigned to Q^4 sites (21).

The ^{29}Si NMR spectrum of the potassium silica gel (KS0.3) is shown in Figure 2. Four main peaks are apparent and attributed to different tetrahedral Q^n environments for Si in silicates. The main fitted peaks are centred at -80 ppm, -88 ppm, -97 ppm and -107 ppm and assigned to Q^1, Q^2, Q^3 and Q^4 sites, respectively (8, 22, 23). The two smaller resonances at -89 ppm and -99 ppm can be assigned to Q^2 and Q^3 sites (24). The fitted relative integral intensities are about 49 % for Q^3, 19 % for Q^2, 16 % for Q^4 and 4 % for Q^1.

The evaluation of the ^{29}Si NMR spectrum of KS0.3 agrees with the band assignments of the Raman spectrum. The four Q units can be determined by both measurement techniques.

Figure 3 shows the Raman spectra for sodium silica gels with different Na/Si molar ratios. All recorded Raman spectra exhibit a strong vibrational band in the range of 2500 – 3750 cm^{-1}. The band position around 3420 cm^{-1} corresponds to OH stretching vibration of H_2O (18). The results for KS0.3 and NS0.3 are almost identical. Therefore, the results for NS0.3 will not be discussed further. The main Raman peak of the sample NS0.6 in the Si-O-Si range (400 – 750 cm^{-1}) appears at 600 cm^{-1} and is linked to SB vibration of Q^2 sites. There is a peak shoulder at 548 cm^{-1} which is related to SB vibration of Q^3 sites. In the higher frequency region, there is a pronounced peak at 1042 cm^{-1} which is attributed to SS vibration (Q^3) (25, 26). The peak position at 1065 cm^{-1}, dominant for samples NS0.6 and NS1.2 which is linked to CO_3^{2-} vibration, indicates the presence of trona [$Na_3H(CO_3)_2 \cdot 2H_2O$] (12, 20). The Raman spectrum of the sample NS1.2 contains two main peaks in the lower frequency region: one peak at 600 cm^{-1} related to SB vibration of Q^2 units and one peak at 450 cm^{-1} linked to SB of O_{NBO}-Si-O_{NBO} (15). In the higher frequency region, a pronounced peak occurs at 776 cm^{-1} that is attributed to an internal deformation vibration of Si-O. Another peak is found at 928 cm^{-1} (SS of Q^1) (12, 17).

On comparing the Raman spectra of the sodium silica gels the following trends were determined. The dominant peak in the low frequency region changes from 530 cm^{-1} (Q^3) to 600 cm^{-1} (Q^2) with increasing

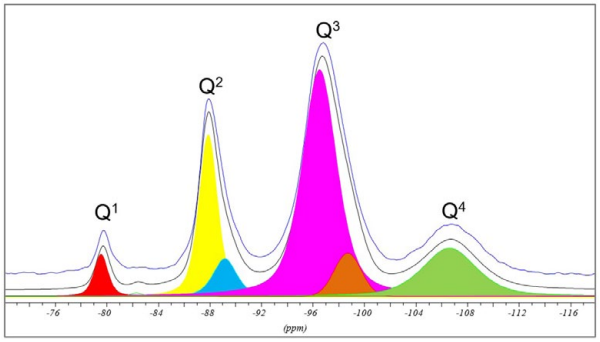

FIGURE 2. ^{29}Si NMR spectrum of the potassium silica gel (K/Si molar ratio = 0.3).

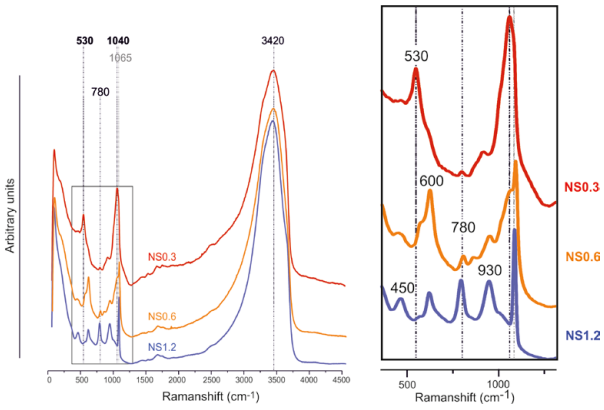

FIGURE 3. Characteristic vibration bands of the sodium silica gels with different Na/Si molar ratios. Left: Raman spectra range 50 – 4500 cm^{-1}, right: enlarged Raman section for the same sodium silica gels.

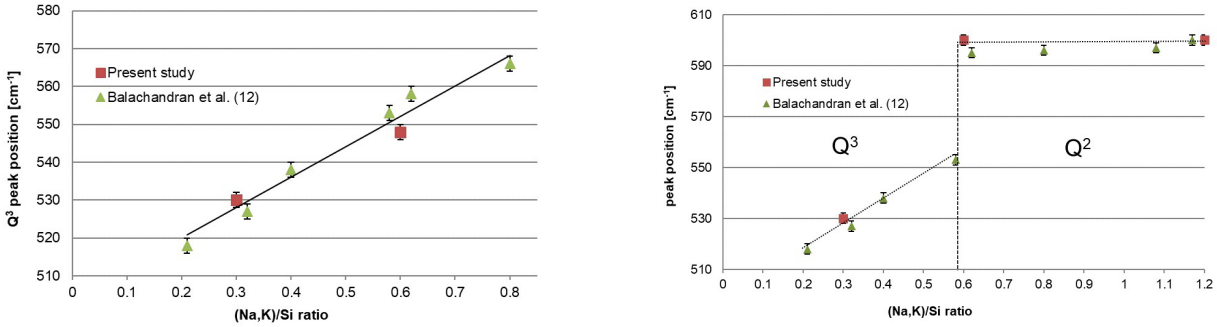

FIGURE 4. Prominent Raman peak position of different ASR gels as a function of (Na,K)/Si molar ratio. Left – linear trend between Q^3 peak position and (Na,K)/Si molar ratio. Right – Relationship between prominent Raman peak position and (Na,K)/Si molar ratio (12).

Na/Si molar ratio. The dominant vibrational band at 530 cm^{-1} for the sample NS0.3 disappears in the case of the sample NS0.6 and a shoulder at 548 cm^{-1} (Q^3) remains. This shoulder linked to Q^3 sites then disappears in the spectrum of NS1.2.

It is also apparent that the Raman peak around 450 cm^{-1} becomes more prominent with increasing Na/Si molar ratio. This indicates an increasing amount of non-bridging oxygen (NBO) and hence a decreasing degree of cross-linking in dependence of the sodium content. The internal deformation vibration band of Si-O at approximately 780 cm^{-1} increases in intensity. Another indication for the decrease in silicate linkage with increasing Na/Si ratio is the intensity increase of the Raman band around 930 cm^{-1} (Q^1). The vibrational band at 430 cm^{-1} (Q^4), similar to that of KS0.3 in Figure 1, is not present in the Raman spectra of the samples NS0.6 and NS1.2.

The main vibrational band in the high frequency region in the spectrum of sample NS0.3 at 1040 cm^{-1} (Q^3) disappears with increasing Na/Si molar ratio; only a sharp Raman peak remains at 1065 cm^{-1}, indicating the presence of trona, in the case of the sample NS1.2. In the Raman spectrum of the gel sample NS0.6, a shoulder, corresponding to SS vibration of Q^3 sites, is still apparent. This shoulder disappears in the spectrum of NS1.2 and only a shallow peak shoulder at 994 cm^{-1} (Q^2) remains. The peak at 928 cm^{-1} (Q^1) emerges as new prominent Raman band. Accordingly, the high-frequency prominent Raman band shifts with increasing Na/Si molar ratio to lower wavenumbers. The carbonate band around 1065 cm^{-1} is sharper at higher Na/Si molar ratios.

In Figure 4, the position of the prominent peak of the Raman spectra with varying (Na,K)/Si molar ratio is shown including results of synthetic ASR gels of Balachandran et al. (12). A linear trend between the Q^3 peak position in Raman spectra and the (Na,K)/Si molar ratio is apparent (Figure 4, left). With increasing (Na,K)/Si molar ratio from 0.2 – 0.8 the peak position of Q^3 shifts from 520 cm^{-1} to 565 cm^{-1}. In Figure 4, the relationship between the prominent peak positions and the (Na,K)/Si molar ratios is shown. The prominent peak position of the sodium and potassium silica gels changes from Q^3 to Q^2 with increasing (Na,K)/Si molar ratio.

3.2. Synthetic sodium-calcium silica gels

The Raman spectra of the sodium-calcium silica gels are compared with a Raman spectrum of a C-S-H phase in Figure 5. The C-S-H phase was synthesized in a previous study with a Ca/Si molar ratio of 0.8 (C-S-H_0.8) (27). Both synthetic ASR gels exhibit a vibrational band at 780 cm^{-1} which corresponds to an internal deformation vibration of Si-O (12). The sharp vibrational band at 1065 cm^{-1} indicates the presence of trona (20).

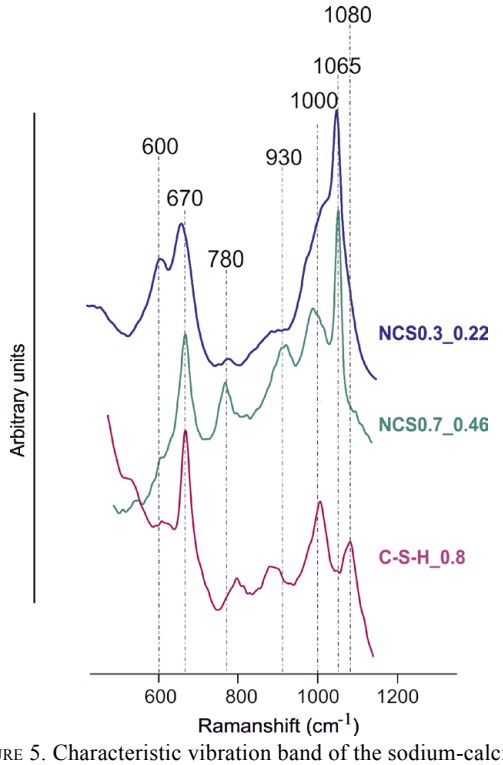

FIGURE 5. Characteristic vibration band of the sodium-calcium silica gels in comparison with C-S-H phase (Ca/Si = 0.8).

The characteristic vibrational bands of the sodium-calcium silica gel NSC0.3_0.22 in the low frequency region are at around 600 cm^{-1} and 660 cm^{-1} (12, 19). The exact assignment of the peak at 600 cm^{-1} is not possible. This Raman peak can be linked to SB of Si-O-Si in Q^3 or Q^2 sites. The present ^{29}Si NMR spectroscopic studies indicate that Q^3 sites dominate the structure of the sample NSC0.3_0.22. Based on the relative integral intensities, the NMR Q^3:Q^2 ratio is roughly 5:3. According to studies (1, 16) on C-S-H phases, the Q^3 peak lies within a range of 594 - 628 cm^{-1}. The peak around 660 cm^{-1} is at a characteristic position for chain silicates as in the case of C-S-H phases (18). Evaluation of the vibrational band reveals a peak around 584 cm^{-1}, which is presumably related to Q^3 sites. The high frequency region contains a peak shoulder at 983 cm^{-1}, linked to SS of Q^2 sites and a peak at 1027 cm^{-1}, which probably linked to Q^3 sites. Due to overlap of the prominent trona vibrational band, band assignment is difficult here. The prominent peak of the sodium-calcium silica gel NSC0.7_0.46 is at 670 cm^{-1}. This peak position is linked to SB of Q^2 sites. A shoulder around 600 cm^{-1} is linked to SB vibration of Si-O-Si and presumably due to Q^3 sites. A broad Raman peak around 772 cm^{-1} is explained by an internal deformation vibration of Si-O. In the higher frequency region, two shallow peaks occur at 932 cm^{-1} and 996 cm^{-1}, which are attributed to SS vibration of Q^1 and Q^2 sites, respectively (12, 16).

As mentioned above, a synthetic C-S-H phase with a Ca/Si molar ratio of 0.8 was measured for comparison purposes. The dominant vibration bands are at 669 cm^{-1} and 1006 cm^{-1} corresponding to SB of Si-O-Si and SS of Si-O, respectively, in Q^2 sites (18). The origin of the vibrational Raman band at 798 cm^{-1} is not certain. According to Black et al. (19), this peak is due to the translation motion of Si compared with O in Q^4 units. The Raman peak at 890cm^{-1} is related to SS of Si-O in Q^1 units. The vibrational band at 1081 cm^{-1} is linked to SS of CO_3^{2-} and indicates the presence of calcium carbonate (15).

The comparison of the two different sodium-calcium silica gels shows a shift of the dominant Raman peak in the low frequency region from 600 cm^{-1} to 670 cm^{-1}. In the Raman spectrum of NSC0.7_0.46 the vibration band at 600 cm^{-1} almost disappears and a dominate peak at 670 cm^{-1} emerges. In the high frequency region, the dominant peak around 1030 cm^{-1} shifts to lower wavenumbers around 1000 cm^{-1} with increasing Ca/Si molar ratio (from 0.22 to 0.46). It is concluded that the main vibrational band position of the sodium-calcium silica gels in the Raman spectra shifts from a Q^3 position with increasing calcium content towards a Q^2 position. The shifts of dominant Raman bands with changing Ca/Si molar ratio point to a structural change in the ASR gel. In particular, the structure of the ASR gel becomes more like that of C-S-H phases, a change which has also been suggested by other authors (28-30).

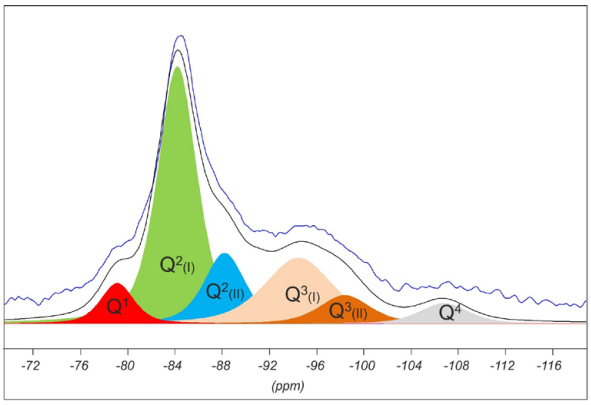

FIGURE 6. ^{29}Si NMR spectrum of the sodium-calcium silica gel NSC0.7_0.46.

^{29}Si NMR spectroscopic investigations on synthetic ASR products by Hou et al. (30) and Leemann et al. (2) have shown that in the presence of calcium new Raman bands occur corresponding to Q^1 and Q^2 sites as in C-S-H phases. The Raman spectra of sodium-calcium silica gels and the C-S-H phase both possess bands around 670 cm^{-1} and 1000 cm^{-1}. Differences in the spectra are for the band position at 800 cm^{-1} (in C-S-H gel) and 780 cm^{-1} (in N-S-C gel). The Q^1 position of the C-S-H phase is at around 890 cm^{-1}, whereas this band occurs at 930 cm^{-1} in the case of N-S-C gels.

Figure 6 shows the ^{29}Si NMR spectrum of the sample NSC0.7_0.46. The characteristic resonances at -79 ppm, -84 ppm, -88 ppm and -95 ppm correspond to Q^1, $Q^2_{(I)}$, $Q^2_{(II)}$, and $Q^3_{(I)}$ sites of silicate tetrahedra (22, 31). The resonances at -99 ppm and -107 ppm can be assigned to $Q^3_{(II)}$ and Q^4 sites (24). The assignments of the two different resonances for Q^2 and Q^3 can be explained by different chemical environments. Depending on the =Si-O counter ion (e.g. Ca^{2+}, Na^+), a chemical shift occurs due to different shielding effects (32). The resonance at -84 ppm ($Q^2_{(I)}$) can also indicate that a C-S-H phase is present (33). However, in this study there is only one peak for pairing or bridging positions, the second peak for a C-S-H dreierkette is missing here. This suggests that the ASR gel is not in coexistence with a C-S-H gel, but becoming as a whole structurally more like that of a C-S-H phase.

4. CONCLUSIONS

The structure of synthetic potassium, sodium and calcium-sodium silicate gels was investigated using Raman and ^{29}Si NMR spectroscopy. The Raman spectroscopic investigations on the ASR gels reveal a change of prominent peak position depending on the (Na+K)/Si and Ca/Si molar ratios. The experiments with sodium silicate gels revealed a shift of the low frequency band from 530 cm^{-1} (Q^3)

to 600 cm^{-1} (Q^2) with increasing Na/Si molar ratio. Moreover, the results show that increasing the Na/Si molar ratio leads to more non-bridging oxygen atoms in the structure and therefore a reduction in the degree of cross-linking. The Q^3 peak position of the sodium silicate gels (Na/Si ratios 0.2 - 0.8) in the Raman spectra (520 - 565 cm^{-1}) can be used to estimate the Na/Si molar ratio of the gel. The low frequency band of the sodium-calcium silica gels shifts towards higher wavenumbers and, with increasing Ca/Si molar ratios, becomes more like that of C-S-H phases. The ^{29}Si NMR investigations confirm the Raman spectroscopic results and indicate local environments similar to those of C-S-H phases for the sodium-calcium gels. Thus, from the overall evaluation, it can be concluded that Raman spectroscopy is a useful analytical method to gain new insights into Q^n species present in the ASR gel structure. The systematic analysis of synthetic ASR gels provides new information on the role of alkalis within the structure of ASR gels.

ACKNOWLEDGMENTS:

The authors thank the German Research Foundation (project number: 438217913) for financially supporting this work.

AUTHOR CONTRIBUTIONS:

Conceptualization: M.E. Krüger, V. Thome. Data curation: M.E. Krüger, M. Kaliwoda. Formal analysis: M.E. Krüger. Funding acquisition: V. Thome. Investigation: M.E. Krüger, H. Hilbig. Methodology: M.E. Krüger, M. Kaliwoda, H. Hilbig. Project administration: M.E. Krüger, H. Hilbig. Resources: M.E. Krüger, V. Thome. Software: M.E. Krüger, V. Thome. Supervision: M. Kaliwoda, H. Hilbig, D. Heinz. Validation: M.E. Krüger, M. Kaliwoda, D. Heinz. Visualization: M.E. Krüger, H. Hilbig. Writing, original draft: M.E. Krüger, M. Kaliwoda, H. Hilbig. Writing, review & editing: M.E. Krüger, V. Thome, M. Kaliwoda, H. Hilbig, D. Heinz.

REFERENCES

1. Leemann, A. (2017) Raman microscopy of alkali-silica reaction (ASR) products formed in concrete. *Cem. Concr. Res.* 102, 41-47. https://doi.org/10.1016/j.cemconres.2017.08.014.
2. Leemann, A.; Shi, Z.; Lindgård, J. (2020) Characterization of amorphous and crystalline ASR products formed in concrete aggregates. *Cem. Concr. Res.* 137, 106190. https://doi.org/10.1016/j.cemconres.2020.106190.
3. Dähn, R.; Arakcheeva, A.; Schaub, P.; Pattison, P.; Chapuis, G.; Grolimund, D.; Wieland, E.; Leemann, A. (2016) Application of micro X-ray diffraction to investigate the reaction products formed by the alkali–silica reaction in concrete structures. *Cem. Concr. Res.* 79, 49-56. https://doi.org/10.1016/j.cemconres.2015.07.012.
4. Geng, G.; Shi, Z.; Leemann, A.; Borca, C.; Huthwelker, T.; Glazyrin, K.; Pekov, I.V.; Churakov, S.; Lothenbach, B.; Dähn, R.; Wieland, E. (2020) Atomistic structure of alkali-silica reaction products refined from X-ray diffraction and micro X-ray absorption data. *Cem. Concr. Res.* 129, 105958. https://doi.org/10.1016/j.cemconres.2019.105958.
5. Shi, Z.; Geng, G.; Leemann, A.; Lothenbach, B. (2019) Synthesis, characterization, and water uptake property of alkali-silica reaction products. *Cem. Concr. Res.* 121, 58-71. https://doi.org/10.1016/j.cemconres.2019.04.009.
6. Shi, Z.; Leemann, A.; Rentsch, D.; Lothenbach, B. (2020) Synthesis of alkali-silica reaction product structurally identical to that formed in field concrete. *Mater. Des.* 190, 108562. https://doi.org/10.1016/j.matdes.2020.108562.
7. Leemann, A.; Shi, Z.; Wyrzykowski, M.; Winnefeld, F. (2020) Moisture stability of crystalline alkali-silica reaction products formed in concrete exposed to natural environment. *Mater. Des.* [195], 109066. https://doi.org/10.1016/j.matdes.2020.109066.
8. Hou, X.; Kirkpatrick, R.J.; Struble, L.J.; Monteiro, P.J.M. (2005) Structural investigations of alkali silicate gels. *J. Am. Ceram. Soc.* 88 [4], 943-949. https://doi.org/10.1111/j.1551-2916.2005.00145.x.
9. Hou, X.; Struble, L.J.; Kirkpatrick, R.J. (2004) Kanemite as a model for asr gel. 12. International Conference on Alkali-Aggregate Reaction in Concrete. Beijing, China, 115-123.
10. Kirkpatrick, R.J.; Kalinichev, A.G.; Hou, X.; Struble, L. (2005) Experimental and molecular dynamics modeling studies of interlayer swelling: water incorporation in kanemite and ASR gel. *Mater. Struct.* 38, 449-458. https://doi.org/10.1007/BF02482141.
11. Mansfeld, T. (2008) The swelling behaviour of alkali silicate gels considering their composition. Bauhaus-Universität Weimar, Dissertation.
12. Balachandran, C.; Muñoz, J.F.; Arnold, T. (2017) Characterization of alkali silica reaction gels using Raman spectroscopy. *Cem. Concr. Res.* 92, 66-74. https://doi.org/10.1016/j.cemconres.2016.11.018.
13. Ling, T.C.; Balachandran, C.; Muñoz, J.F.; Youtcheff, J. (2018) Chemical evolution of alkali-silicate reaction (ASR) products: a Raman spectroscopic investigation. *Mater. Struct.* 51, 23. https://link.springer.com/article/10.1617%2Fs11527-018-1151-x.
14. Drozdovskiy, I.; Ligeza, G.; Jahoda, P; Franke, M.; Lennert, P.; Vodnik, P.; Payler, S.J.; Kaliwoda, M.; Pozzobon, R.; Massironi, M.; Turchi, L.; Bessone, L.; Sauro, F. (2020) The PANGAEA Mineralogical Database. *Data Br.* 31, 105985. https://doi.org/10.1016/j.dib.2020.105985.
15. Black, L. (2009) Raman spectroscopy of cementitious materials. In Spectrosc. Prop. Inorg. Organomet. Compd., J. Yarwood; Douthwaite, R.; Duckett, S. B. https://doi.org/10.1039/b715000h.
16. Garbev, K.; Stemmermann, P.; Black, L.; Brenn, C.; Yarwood, J.; Gasharova, B. (2007) Structural features of C–S–H(I) and its carbonation in air—A Raman spectroscopic study. Part I: fresh phases. *J. Am. Ceram. Soc.* 90, 900-907. https://doi.org/10.1111/j.1551-2916.2006.01428.x.
17. McMillan, P. (1984) Structural studies of silicate glasses and melts - applications and limitations of Raman spectroscopy. Am. Min. 69, 622-644.
18. Higl, J.; Köhler, M.; Lindén, M. (2016) Confocal Raman microscopy as a non-destructive tool to study microstructure of hydrating cementitious materials. *Cem. Concr. Res.* 88, 136-143. https://doi.org/10.1016/j.cemconres.2016.07.005.
19. Black, L.; Breen, C.; Yarwood, J.; Garbev, K.; Stemmermann, P.; Gasharova, B. (2007) Structural features of C–S–H(I) and its carbonation in air—A Raman spectroscopic study. Part II: carbonated phases. *J. Am. Ceram. Soc.* 90, 908-917. https://doi.org/10.1111/j.1551-2916.2006.01429.x.
20. Hurai, V.; Huraiová, M.; Slobodník, M.; Thomas, R. (2015) Geofluids, 1st Edition, Elsevier, https://doi.org/10.1016/C2014-0-03099-7.
21. Ortaboy, S.; Li, J.; Geng, G; Myers, R.J.; Monteiro, P.J.M.; Maboudian, R.; Carraro, C. (2017) Effects of CO_2 and temperature on the structure and chemistry of C–(A–)S–H investigated by Raman spectroscopy. *RSC Adv.* 7 [77], 48925-48933. https://doi.org/10.1039/C7RA07266J.
22. Tambelli, C.E.; Schneider, J.F.; Hasparyk, N.P.; Monteiro, P.J.M. (2006) Study of the structure of alkali-silica reaction gel by high-resolution NMR spectroscopy. *J. Non. Cryst. Solids.* 353 [32-35], 3429-3436. https://doi.org/10.1016/j.jnoncrysol.2006.03.112.
23. Walkley, B.; Provis, J.L. (2019) Solid-state nuclear magnetic resonance spectroscopy of cements. *Mater. Today Adv.* 1, 100007. https://doi.org/10.1016/j.mtadv.2019.100007.

24. Dedecek, J.; Balgová, V.; Pashkova, V.; Klein, P.; Wichterlová, B. (2012) Synthesis of ZSM-5 Zeolites with defined distribution of al atoms in the framework and multinuclear MAS NMR analysis of the control of Al distribution. *Chem. Mater.* 24 [16], 3231–3239. https://doi.org/10.1021/cm301629a.
25. Huang, Y.; Jiang, Z.; Schwieger, W. (1998) A vibrational study of kanemite. *Micropo. Mesopo. Mat.* 26, 215-219. https://doi.org/10.1016/S1387-1811(98)00270-4.
26. Kalampounias, A.G. (2011) IR and Raman spectroscopic studies of sol-gel derived alkaline-earth silicate glasses. *Bull. Mater. Sci.* 34, 299-303. https://doi.org/10.1007/s12034-011-0064-x.
27. Irbe, L.; Beddoe, R.E.; Heinz, D. (2019) The role of aluminium in C-A-S-H during sulfate attack on concrete. *Cem. Concr. Res.* 116, 71–80. https://doi.org/10.1016/j.cemconres.2018.11.012.
28. Cong, X.D.; Kirkpatrick, R.J.; Diamond, S. (1993) ^{29}Si MAS NMR spectroscopic investigation of alkali silica reaction product gels. *Cem. Concr. Res.* 23 [4], 811-823. https://doi.org/10.1016/0008-8846(93)90035-8.
29. Leemann, A.; Le Saout, G.; Winnefeld, F.; Rentsch, D.; Lothenbach, B. (2011) Alkali–silica reaction: the influence of calcium on silica dissolution and the formation of reaction products. *J. Am. Ceram. Soc.* 94 [4], 1243-1249. https://doi.org/10.1111/j.1551-2916.2010.04202.x.
30. Hou, X.; Struble, L.J.; Kirkpatrick, R.J. (2004) Formation of ASR gel and the roles of C-S-H and portlandite. *Cem. Concr. Res.* 34 [9], 1683-1696. https://doi.org/10.1016/j.cemconres.2004.03.026.
31. Lothenbach, B.; Nied, D.; L´Hôpital, E.; Achiedo, G.; Dauzéres, A. (2015) Magnesium and calcium silicate hydrates. *Cem. Concr. Res.* 77, 60-68. https://doi.org/10.1016/j.cemconres.2015.06.007.
32. Myers, R.J.; Bernal, S.A.; Gehman, J.D.; van Deventer, J. S.J.; Provis, J.L. (2015) The role of Al in cross-linking of alkali-activated slag cements. *J. Am. Ceram. Soc.* 98 [3], 996-1004. https://doi.org/10.1111/jace.13360.
33. Sevelsted, T.F; Skibsted, J. (2015) Carbonation of C–S–H and C–A–S–H samples studied by ^{13}C, ^{27}Al and ^{29}Si MAS NMR spectroscopy. *Cem. Concr. Res.* 71, 56-65. https://doi.org/10.1016/j.cemconres.2015.01.019.